Forward M-ary Hypothesis Testing Based Detection Approach for Passive Radar

Amir Zaimbashi

***Abstract*—In contrast to active radar systems, in which the transmitted waveforms are carefully selected and designed in relation to the radar operational modes and requirements, passive radars(PRs) exploiting non-cooperative illuminators of opportunity need to cope with waveforms that are not tailored for the radar applications. In the latter case, it is likely that target echoes are masked by echoes from other strong targets in multi-target scenarios. This fact inspired us to model the multi-target detection problem in the PRs as an M-ary hypothesis testing problem. We then employ the generalized likelihood ratio (GLR) principle to derive the GLR-based detector. A parallel and recursive implementation of the detector is presented for computationally efficient implementation, in which the targets are detected sequentially and the previously detected targets are treated as interferences to be removed yielding the detection of the weakest ones. The false alarm and detection performance of the proposed sequential GLR-based detector are analytically studied using asymptotic distribution and also their accuracies are verified numerically. Simulation results show that there is a high agreement between asymptotic performance and the one obtained by simulation results. Extensive simulation results for both FM and DVB-T based passive radars are presented to demonstrate the effectiveness of the proposed detection algorithm. Furthermore, it can be revealed from our simulation results that the proposed detection algorithm significantly outperforms the existing methods without adding significant complexity to them.**

***Index Terms*—Passive radar, M-ary hypothesis testing problem, generalized likelihood ratio test, FM and DVB-T opportunity signals.**

I. INTRODUCTION

PAssive radar (PR) systems have received a growing interest over the last decade, which use signals of such as analogue television (TV) [1], frequency modulated (FM) commercial radio [2], digital video broadcast-terrestrial (DVB-T) [3]–[5], digital audio broadcast (DAB) [6], global system for mobile communications (GSM) [7], and long-term evolution (LTE) [8], as illuminators for target detection, localization, and tracking. Broadly speaking, arguments for the selection of an opportunity transmitter include spatial and time coverage, transmitter power, transmitter central frequency, bandwidth of broadcast signals, shape of the ambiguity function and so on. More precisely, the bandwidth of a signal dictates the achievable range-resolution, the shape of the ambiguity function is crucial in determining the detection performance of a PR system, and the others parameters can affect the coverage diagram of a PR. In the case of digital broadcast signals, DVB-T signals generally offer a close-to-ideal ambiguity function for target detection, but it often have low power transmitters. Among all the emitters available in the environment, however, the commercial FM radio stations offer a good tradeoff between performance and overall system development costs [9]-[11].

It is known that the detection and localization performance of a radar system depend on the transmitted waveform. Unfortunately, the characteristics of the transmitted waveform in a PR system are not under the control of a radar designer; moreover, these characteristics can unpredictably change with time. This is clearly the case with the transmitted FM radio waveforms, which result in a PR ambiguity function with usually time-varying characteristics, involving both range resolution and sidelobe level, which exist at a level not much lower than that of mainlobe. In the case of DVB-T signal, the presence of specific features such as guard intervals and pilot subcarriers in the orthogonal frequency division multiplexing (OFDM) modulation yields in a number of undesired peaks in the corresponding ambiguity function [12]. This behavior of waveforms that are not tailored for radar applications leads to the greatest limitation of a PR system known as the masking effect of nuisance signals, including the direct signal, multipath/clutter echoes and strong targets echoes, for the weakest targets present in a considered scenario [10]- [19]. In addition, this might be the cause for increasing actual false alarm rate and thus significantly limit the detection capability of a PR system. This standpoint clears the key distinction between target detection in active radar and that of passive one, which necessitates considering both the presence of the receiver noise and clutter echoes in the PR detection problem as well as the presence of the direct path signal and interfering targets in a multi-target detection problem.

In a bistatic framework, a number of passive target detection approaches have been studied in the literature [5]- [19]. With the exception of [11] and our previous works [14]- [19], most of the existing literature ignores the detrimental effect of stronger targets on the weak ones and develops some detectors based on the single-target assumption. Also, the works in [21]-[25] focus on passive radar imaging of moving targets or target detection problem in a multistatic framework. In this case, authors of [24] and [25] also ignored the harmful effect of clutter and interfering target signals on the calculation and analysis of their detectors in passive multiple-input multiple-output (MIMO) radar networks and passive multistatic radar, respectively. In our previous works presented in [14]- [19], we formulated the target detection problem in single- and

Manuscript received , 2016; revised ?, 2016. Date of publication February ?, 2017; date of current version ?, 2017. The associate editor coordinating the review of this paper and approving it for publication was Dr. Fauzia Ahmad.

The author is with the Department of Electrical Engineering, Shahid Bahonar University of Kerman, Kerman, Iran. Email: a.zaimbashi@uk.ac.ir

Color versions of one or more of the figures in this paper are available online at ?.

Digital Object Identifier ?

multi-band FM-based bistatic PR system as a composite and binary hypothesis testing problem in the presence of above nuisance signals, in which a two-step generalized likelihood ratio (GLR)-based detector was suggested. To implement the GLR test, interfering targets delay-Doppler coordinates should be estimated, so it would be a two step GLR (2S-GLR)-based detector. In the first step of the 2S-GLR-based detector, a heuristic algorithm referred to as imperative target positioning (ITP) algorithm has been developed to estimate the Doppler-range coordinate of the interfering targets. In the second step, one target is considered as the target under test and others are considered as the interfering targets to regulate the false alarm of the proposed detector. Simulation results of [14]-[16] showed that the 2S-GLR based detector significantly outperforms the detectors presented in [11]- [13]. In contrast to our previous works, here, we model the single- channel target detection problem as an M-ary hypothesis testing problem. To solve this new detection problem, we consider the M-ary hypothesis testing problem as a series of binary hypothesis testing problem and propose a forward and sequential GLR-based detector. Compared with our previous works [14]- [19], our main contributions are as follows:

- To cope with the severe masking effect of strong targets on the weak ones or increasing the false alarm rate, for the first time, we model the target detection problem in a bistatic PR system as an M-ary hypothesis testing problem, in which targets must be detected one after the other, whereas this problem is modeled as a binary composite hypothesis testing problem in our previous works.
- We propose a forward implementation of GLR-based detector by considering the M-ary hypothesis testing problem as a series of binary hypothesis testing problem. The proposed detection strategy is based on the sequential use of the generalized likelihood ratio test exploited for binary composite case. The obtained binary GLR-based detector differs from the one in our previous works in the sense that it aims at detecting targets with unknown delay-Doppler coordinates, whereas the detectors of our previous works detect the presence of a target in a specific delay-doppler coordinate.
- To reduce the computational complexity and the amount of memory required to implement the proposed detector, a parallel and recursive implementation of the forward GLR-based detector is presented, in which targets from strongest to weakest ones are sequentially detected and the previously detected targets are treated as interferences to be removed thus allowing the detection of the weakest ones.
- In the new derived detector, the false alarm and detection performances of the proposed GLR-based detector are analytically studied using asymptotic distribution, and their accuracies are numerically verified.
- Our previous works focused only on FM radio signals, but the efficacy of the proposed detector for both FM radio and DVB-T signals are considered in this paper. More importantly, this paper also shows that designing a constant false alarm rate (CFAR) detector, with respect to opportunity waveforms used over different processing times, is not easily accessible in an FM-based PR with time-varying waveforms, whereas it is expected for DVB-T-based PR systems with approximately time-invariant waveforms. In this case, it is shown that the proposed detector guarantees a lower false alarm rate than the one used for threshold setting in an FM-based PR system, while it has CFAR property when used for the DVB-T -based PR systems.
- Finally, we show that the proposed detector is simpler than the 2S-GLR-based detector of [15], and thus has lower computational complexity. Furthermore, we compare the performance of the proposed detector with the existing methods in the literature and demonstrate the superiority of the proposed detection algorithm over well-known methods without adding significant complexity to them.

  In the sections to follow, we will discuss these contributions in detail.

In this paper, scalars are denoted by nonboldface lowercase letter, e.g., a. Vectors are denoted by boldface lowercase letters, e.g., $\mathbf{a}$, and matrices by boldface uppercase letters, e.g., $\mathbf{A}$. Superscripts $(.)^T$, $(.)^*$ and $(.)^H$ denote transpose, complex conjugate and complex conjugate transpose, respectively. The Euclidean norm of vector $\mathbf{x}$ is denoted by $\|\mathbf{x}\|$, $|x|$ represents the modulus of x, and the symbol $\odot$ represents the Hadamard elementwise product. Here, $F_{1,N-(P_e+m)}$ denotes a central complex F distribution with 1 numerator complex degree of freedom and $N-(P_e+m)$ denominator complex degree of freedom, and $F_{1,N-(P_e+m)}(\delta_m)$ denotes an noncentral complex F distribution with 1 numerator complex degree of freedom and $N-(P_e+m)$ denominator complex degree of freedom and the non-centrality parameter δ_m. Here, $\mathcal{X}^2_r(\lambda)$ denotes a real complex chi-square distribution with r real degree of freedom and the real non-centrality parameter λ.

II. System Model

Consider a bistatic PR system, in which receiver isolates the direct-path and target-path signals into reference and surveillance channels, respectively. This is accomplished by pointing directional antennas at the transmitter and the anticipated target region, respectively [20]. In a multi-target scenario with M targets, and in the presence of the system thermal noise, direct signal and clutter/multipath returns, the base-band received surveillance signal vector can be compactly described by the following model:

$$\mathbf{x} = \mathbf{Sa} + \mathbf{Hc} + \mathbf{n} \tag{1}$$

where

- $\mathbf{x} \in \mathcal{C}^{N\times 1}$ is the $N \times 1$ vector obtained after sampling a window of the surveillance signal. The size of the window, say T, is called the coherent processing interval(CPI) and determines the Doppler resolution and the processing gain of the system. As such, $N = Tf_s$ with f_s being the sampling frequency.

- Target signal matrix $\mathbf{S}$ is an $N \times M$ matrix defined as:

$$\mathbf{S} \triangleq [\mathbf{s}_1, ..., \mathbf{s}_M], \tag{2}$$

where

$$\mathbf{s}_m = (\mathbf{y}^{(n_m)} \odot \mathbf{e}^{(f_m)}) \tag{3}$$

where (n_m, f_m) represents the delay-Doppler coordinates of the mth targets; $\mathbf{y}^{(n_m)} = \mathbf{P}^{n_m}\mathbf{y}$ where $\mathbf{y}$ is the reference signal after an equalization technique is applied to it to further isolate the direct-path signals received; $\mathbf{P}$ is an $N \times N$ permutation matrix defined as $[\mathbf{P}]_{ij} = 1$ if $i = j + 1$ and 0 otherwise for $i = 0, ..., N-1$; $j = 0, ..., N-1$. Here, $[\mathbf{e}^{(f_m)}]_n = e^{j2\pi f_m n T_s}$ with $n = 0, ..., N-1$; $\mathbf{a} = [\alpha_1, ..., \alpha_M]^T$ is the M-dimensional column vector containing all complex amplitudes of the desired targets.

- Clutter signature matrix $\mathbf{H}$ is an $N \times P$ matrix defined as:

$$\mathbf{H} \triangleq [\mathbf{h}_1, ..., \mathbf{h}_p, ..., \mathbf{h}_P], \tag{4}$$

where $\mathbf{h}_p = (\mathbf{y}^{n_c^{(p)}} \odot \mathbf{e}^{f_c^{(p)}})$ where $n = 0, ..., N-1$. In this case, $n_c^{(p)}$ and $f_c^{(p)}$ are determined based on the delay-Doppler coordinates of the clutter signature for $p = 1, ..., P$; $\mathbf{c} = [c_1, ..., c_P]^T$ is the P-dimensional unknown column vector containing all amplitudes corresponding to any delay-Doppler coordinates of the clutter signature. Since our focus of the present work is on the target detection, we use the clutter model presented in [15], and the interested reader is refereed to it for more detail about clutter modeling.

- $\mathbf{n} \in \mathcal{C}^{N\times 1}$ represents additive Gaussian noise in the surveillance channel of PR system and has the distribution $\mathcal{CN}(0_{N\times 1}, \sigma^2\mathbf{I}_N)$ with unknown variance σ^2.

III. M-ary Hypothesis Testing Based Detection Approach

In a multi-target scenario, since the weak targets are susceptible to masking in presence of other strong targets, even in the presence of large range-Doppler separations, it makes sense to develop a detection strategy, in which targets are detected one after another. To do this, for the first time, we aim to formulate the target-detection problem of PR systems for multi-target scenarios as a composite M-ary hypothesis problem and solve it based on the detection theory framework. Thus, According to the expression for the received signal from (1) to (4), the hypothesis test can be formulated as (5), shown at the top of the next page, where hypothesis $\mathcal{H}_m$ denotes the presence of the mth targets in the presence of the system thermal noise, direct signal and clutter/multipath returns. In (5), we have a set of hypotheses $\mathcal{H}_0 \subset \mathcal{H}_1 ... \subset \mathcal{H}_m \subset ...$, and that each hypothesis specifies a probability density function (pdf) $f_m(\mathbf{x}; \theta_m)$ with a parameter vector θ_m of dimension $L_m = dim(\theta_m|\mathcal{H}_m)$ in the parameter space Θ_m. For the notational convenience we, in the sequel, suppress the subscript m from θ_m and Θ_m but the reader should keep in mind that these differ for each hypothesis. For the mth hypothesis, let

$$\ell_m(\theta; \mathbf{x}) = ln(f_m(\mathbf{x}; \theta)) \tag{6}$$

denote the log-likelihood function of the observation under the mth hypothesis. Generally, the problem of multiple composite hypothesis testing is more difficult than the binary composite case [26]. In the problem at hand, we would like to test the hypotheses sequentially, taking advantage of the fact that as a strong target is detected, we can remove its effect, so that we may be able to detect lower power targets. To do so, we propose a new detection strategy which is based on the sequential use of the generalized likelihood ratio test used for binary composite case. In a binary composite case, the GLRT statistic for testing $\mathcal{H}_m$ against $\mathcal{H}_{m-1}$, defined as [26]

$$\Lambda_m(\mathbf{x}) = 2(\ell_m(\hat{\theta}; \mathbf{x}) - \ell_{m-1}(\hat{\theta}; \mathbf{x})) \underset{\mathcal{H}_{m-1}}{\overset{\mathcal{H}_m}{\gtrless}} \eta_m \tag{7}$$

where the threshold η_m is chosen to satisfy a specified probability of false alarm p_{fa}, and the natural point estimate of θ is the maximum likelihood estimate (MLE) $\hat{\theta} = argmax_{\mathbf{\Theta}_m} \ell_m(\theta; \mathbf{x})$ which is assumed to be unique. By the general maximum likelihood theory, $\Lambda_m(\mathbf{x})$ has $\chi^2_{DOF(m)}$ distribution asymptotically (i.e., chi-squared distribution with DOF(m) degrees of freedom), where

$$DOF(m) = dim(\theta|\mathcal{H}_m) - dim(\theta|\mathcal{H}_{m-1}). \tag{8}$$

where $DOF(m)$ is the number of scalar unknowns that take different values under $\mathcal{H}_m$ and $\mathcal{H}_{m-1}$ [27]. In the sequel, $\mathcal{H}_{m-1}$ ($\mathcal{H}_m$) is referred to as null (alternative) hypothesis, and we will derive Binary Hypothesis GLRT (BH-GLRT)-based detector when testing $\mathcal{H}_m$ against $\mathcal{H}_{m-1}$.

A. Binary Hypothesis GLRT-Based Detector

As mentioned before, in our detection strategy, we consider a series of binary composite hypotheses. For example, to test $\mathcal{H}_m$ against $\mathcal{H}_{m-1}$, we can consider the binary composite hypothesis problem of (9), shown at the top of the next page. We can also express detection problem (9) compactly as

$$\begin{cases} \mathcal{H}_{m-1} : \mathbf{x} = \mathbf{T}_{m-1}\mathbf{g}_{m-1} + \mathbf{H}\mathbf{c} + \mathbf{n}, \\ \mathcal{H}_m : \mathbf{x} = \mathbf{s}_m\alpha_m + \mathbf{T}_{m-1}\mathbf{g}_{m-1} + \mathbf{H}\mathbf{c} + \mathbf{n} \end{cases} \tag{10}$$

where

$$\mathbf{T}_{m-1} = [\mathbf{s}_1, ..., \mathbf{s}_{m-1}] \tag{11}$$

and

$$\mathbf{g}_{m-1} = [\alpha_1, ..., \alpha_{m-1}]^T \tag{12}$$

To test $\mathcal{H}_m$ against $\mathcal{H}_{m-1}$ with the set of unknown parameters

$$\mathbf{\Theta}_m = \{(n_m, f_m), \alpha_m, \mathbf{g}_{m-1}, \mathbf{c}, \sigma^2\} \tag{13}$$

$$\mathbf{\Theta}_{m-1} = \{\mathbf{g}_{m-1}, \mathbf{c}, \sigma^2\}, \tag{14}$$

one can replace the unknown parameters under $\mathcal{H}_{m-1}$ and $\mathcal{H}_m$ with their MLE in the GLRT form presented in (7) to obtain

$$\Lambda_m(\mathbf{x}) = -2N \ln\Big(1 - \max_{(n_m, f_m)} i_m(n_m, f_m)\Big) \underset{\mathcal{H}_{m-1}}{\overset{\mathcal{H}_m}{\gtrless}} \eta_m \tag{15}$$

where

$$i_m(n, f) = \frac{|\mathbf{s}(n, f)^H \mathbf{\Pi}^{\perp}_{\mathbf{U}_{(P+m-1)}} \mathbf{x}|^2}{||\mathbf{\Pi}^{\perp}_{\mathbf{U}_{(P+m-1)}} \mathbf{s}(n, f)||^2 ||\mathbf{\Pi}^{\perp}_{\mathbf{U}_{(P+m-1)}} \mathbf{x}||^2} \tag{16}$$

$$\begin{cases} \mathcal{H}_0 : \mathbf{x} = \mathbf{Hc} + \mathbf{n}, \\ \mathcal{H}_1 : \mathbf{x} = \mathbf{s}_1\alpha_1 + \mathbf{Hc} + \mathbf{n}, \\ \mathcal{H}_2 : \mathbf{x} = \mathbf{s}_2\alpha_2 + \mathbf{s}_1\alpha_1 + \mathbf{Hc} + \mathbf{n}, \\ \mathcal{H}_3 : \mathbf{x} = \mathbf{s}_3\alpha_3 + [\mathbf{s}_1, \mathbf{s}_2][\alpha_1, \alpha_1]^T + \mathbf{Hc} + \mathbf{n}, \\ \vdots \quad : \qquad\qquad\qquad \vdots \\ \mathcal{H}_m : \mathbf{x} = \mathbf{s}_m\alpha_m + [\mathbf{s}_1, ..., \mathbf{s}_{m-1}][\alpha_1, ..., \alpha_{m-1}]^T + \mathbf{Hc} + \mathbf{n}, \\ \vdots \quad : \qquad\qquad\qquad \vdots \end{cases} \tag{5}$$

$$\begin{cases} \mathcal{H}_{m-1} : \mathbf{x} = \mathbf{s}_{m-1}\alpha_{m-1} + [\mathbf{s}_1, ..., \mathbf{s}_{m-2}][\alpha_1, ..., \alpha_{m-2}]^T + \mathbf{Hc} + \mathbf{n}, \\ \mathcal{H}_m : \mathbf{x} = \mathbf{s}_m\alpha_m + [\mathbf{s}_1, ..., \mathbf{s}_{m-1}][\alpha_1, ..., \alpha_{m-1}]^T + \mathbf{Hc} + \mathbf{n}. \end{cases} \tag{9}$$

where

$$\mathbf{\Pi}^{\perp}_{\mathbf{U}_{(P+m-1)}} = \mathbf{I} - \mathbf{U}_{(P+m-1)}(\mathbf{U}^H_{(P+m-1)}\mathbf{U}_{(P+m-1)})^{-1}\mathbf{U}^H_{(P+m-1)} \tag{17}$$

Here, the interference matrix $\mathbf{U}_{(P+m-1)}$ is defined as $\mathbf{U}_{(P+m-1)} = [\mathbf{H}, \mathbf{T}_{m-1}]$ where $\mathbf{U}_{(P)} = \mathbf{H}$[1]. We see that the direct signal, clutter and the previously detected targets are treated as interferences in the the interference matrix $\mathbf{U}_{(P+m-1)}$ to be removed thus allowing the detection of mth target (if exist). In order to determine the value of the threshold η_m, it is shown in [15] that

$$\Upsilon_m(\mathbf{x}) = \frac{\frac{i_m(n_m,f_m)}{1}}{\frac{1-i_m(n_m,f_m)}{N-(P+m)}} \sim \begin{cases} F_{1,N-(P+m)} & under\ \mathcal{H}_{m-1} \\ F_{1,N-(P+m)}(\delta_m) & under\ \mathcal{H}_m \end{cases} \tag{18}$$

where (n_m, f_m) is the true delay-Doppler coordinate of mth target under test, and $\delta_m = \frac{|\alpha_m|^2}{\sigma^2}\|\mathbf{\Pi}^{\perp}_{\mathbf{U}_{(P+m-1)}}\mathbf{s}(n_m, f_m)\|^2$. In order to give a desired integration gain in PR systems, N gets a large value, so $F_{1,N-(P+m)}$ and $F_{1,N-(P+m)}(\delta_m)$ tend to the complex χ^2_1 and $\chi^2_1(\delta_m)$, respectively. Note that $i_m(n_m, f_m)$ gets value close to zero under $\mathcal{H}_{m-1}$ hypothesis, so we can approximate $-2N\ln\big(1-\max_{(n_m,f_m)} i_m(n_m, f_m)\big)$ with $2N\max_{(n_m,f_m)} i_m(n_m, f_m)$. Hence, the GLRT of (15) is asymptotically equivalent to

$$\lambda_m(\mathbf{x}) = 2N \max_{(n_m,f_m)} i_m(n_m, f_m) \underset{\mathcal{H}_{m-1}}{\overset{\mathcal{H}_m}{\gtrless}} \eta_m \tag{19}$$

Note that, for decision-making with the statistic $\Upsilon_m(\mathbf{x})$, we compare $\Upsilon_m(\mathbf{x})$ against a threshold, denoted here by η. From (18) and (19), one can obtain that $\eta_m = \frac{N\eta}{N-(P+m)-\eta}$. Under the large values of N, which is typical in PR systems, this threshold may be approximated by η. As one can notice, the threshold η_m does not depend on m. This means that the threshold of the proposed detector does not depend on the maximum number of targets to be detected under hypothesis $\mathcal{H}_m$, say m. Thus, in the sequel, we denote η_m by η.

In essence the proposed detector decides that a new target with respect to that of hypothesis $\mathcal{H}_{m-1}$ is present, say mth target, if the peak value of $i_m(n_m, f_m)$ exceed a threshold, and if so, the delay-Doppler coordinate of that peak is the MLE of the target delay-Doppler coordinate denoting by $(\hat{n}_m, \hat{f}_m)$. When (n_m, f_m) is known, the GLRT of (19) becomes

$$\lambda'_m(\mathbf{x}) = 2Ni_m(n_m, f_m) \underset{\mathcal{H}_{m-1}}{\overset{\mathcal{H}_m}{\gtrless}} \eta' \tag{20}$$

It is not difficult to show that, for large values of N, $2Ni_m(n_m, f_m) \sim \mathcal{X}^2_2$ and $2Ni_m(n_m, f_m) \sim \mathcal{X}^2_2(2\delta_m)$ under $\mathcal{H}_{m-1}$ and $\mathcal{H}_m$ hypotheses, respectively. In this case, the threshold η' is chosen to satisfy

$$p'_{fa} = Pr\big\{2Ni_m(n_m, f_m) > \eta' | \mathcal{H}_{m-1}\big\} = e^{-0.5\eta'} \tag{21}$$

It should be noted that p'_{fa} is the probability of false alarm if we examine known delay-Doppler bin (n_m, f_m). In the case of unknown (n_m, f_m) and for large values of N, the only difference is that the false alarm probability increases approximately linearly with the number of delay-Doppler coordinates searched over [26]. Henceforth, the corresponding threshold, η, based on test statistic $\lambda_m(\mathbf{x})$ is derived as

$$p_{fa} = \zeta D_d e^{-0.5\eta} \tag{22}$$

where D_d is the number of delay-Doppler coordinates searched over, and ζ is a value less than one. Generally speaking, parameter ζ takes different values according to the characteristics of the opportunity signals used over different CPIs. In simulation section, we will discuss the selection of parameter ζ in more detail.

B. Forward and Recursive Implementation of the BH-GLRT-Based Algorithm

In the proposed multi-target detection algorithm, we first test $\mathcal{H}_1$ against $\mathcal{H}_0$, if it is accepted by the BH-GLRT statistic, i.e., $\lambda_1(\mathbf{x}) > \eta$ for some predetermined false alarm probability, then test $\mathcal{H}_2$ against $\mathcal{H}_1$, etc. until the first rejection, i.e., until $\lambda_m(\mathbf{x}) < \eta$. More precisely, the sequence of hypotheses ($\mathcal{H}_0$, $\mathcal{H}_1$), ($\mathcal{H}_1$, $\mathcal{H}_2$), ...,($\mathcal{H}_{m-1}$, $\mathcal{H}_m$), ($\mathcal{H}_m$, $\mathcal{H}_{m+1}$), ..., ($\mathcal{H}_M$, $\mathcal{H}_{M+1}$) from the direct direction are tested to find new targets in the proposed detector. For instance, if $\mathcal{H}_m$ is accepted when testing $\mathcal{H}_m$ against $\mathcal{H}_{m-1}$, a new target (mth target) is declared as detected and the test procedure proceeds to the next hypothesis to test $\mathcal{H}_{m+1}$ against $\mathcal{H}_m$. It stops when the $\mathcal{H}_{m-1}$ hypothesis is accepted, implying that no further

[1]Note that (m-1) is the number of interfering targets been detected.

target can be detected. The number of targets, say M, is then estimated by the dimension of the signal vector under the accepted null hypothesis. We call this as Forward M-ary hypothesis testing strategy. In the following, we implement this target-detection strategy in a recursive manner to use some of previous computations in order to reduce computational complexity of proposed detector. To do so, we first rewrite (16) as

$$i_m(n,f) = \frac{|\mathbf{s}(n,f)^H \mathbf{x}^{\perp(P+m-1)}|^2}{\|\mathbf{p}\|^2 \|\mathbf{x}^{\perp(P+m-1)}\|^2} \tag{23}$$

where

$$\mathbf{p} = \mathbf{\Pi}^{\perp}_{\mathbf{U}_{(P+m-1)}} \mathbf{s}(n,f) \tag{24}$$

where $\mathbf{x}^{\perp(P+m-1)} = \mathbf{\Pi}^{\perp}_{\mathbf{U}_{(P+m-1)}} \mathbf{x}$ represents the component of $\mathbf{x}$ orthogonal to the space spanned by the columns of $\mathbf{U}_{(P+m-1)}$. Hereafter, for simplicity of notation, the interference matrix $\mathbf{U}_{(P+m-1)}$ is written as $\mathbf{U}_{(P+m-1)} = [\mathbf{U}_{(P)}, \mathbf{u}_{P+1}, ..., \mathbf{u}_{P+m-1}]$ where $\mathbf{U}_{(P)} = \mathbf{H}$ and $\mathbf{u}_{P+i} = \mathbf{s}_i$. Using the recursive orthogonal projection of matrix $\mathbf{\Pi}^{\perp}_{\mathbf{U}_{(P+m-1)}}$, given by (for $m \geq 2$) [28]

$$\mathbf{\Pi}^{\perp}_{\mathbf{U}_{(P+m-1)}} = \mathbf{\Pi}^{\perp}_{\mathbf{U}_{(P+m-2)}} - \frac{\mathbf{\Pi}^{\perp}_{\mathbf{U}_{(P+m-2)}} \mathbf{u}_{P+m-1} \mathbf{u}^H_{P+m-1} \mathbf{\Pi}^{\perp}_{\mathbf{U}_{(P+m-2)}}}{\mathbf{u}^H_{P+m-1} \mathbf{\Pi}^{\perp}_{\mathbf{U}_{(P+m-2)}} \mathbf{u}_{P+m-1}} \tag{25}$$

where $\mathbf{U}_{(P+m-1)} = [\mathbf{U}_{(P+m-2)}, \mathbf{u}_{P+m-1}]$, we then update $\mathbf{x}^{\perp(P+m-1)}$ recursively as follows

$$\mathbf{x}^{\perp(P+m-1)} = \mathbf{x}^{\perp(P+m-2)} - \frac{\mathbf{u}^{\perp(P+m-2)}_{P+m-1} \mathbf{u}^{\perp(P+m-2)H}_{P+m-1} \mathbf{x}^{\perp(P+m-2)}}{\|\mathbf{u}^{\perp(P+m-2)}_{P+m-1}\|^2} \tag{26}$$

where $\mathbf{x}^{\perp(P)} = \mathbf{x} - \mathbf{U}_{(P)} \mathbf{R}_P \mathbf{U}^H_{(P)} \mathbf{x}$ with $\mathbf{R}_P = (\mathbf{U}^H_{(P)} \mathbf{U}_{(P)})^{-1}$. Here, $\mathbf{u}^{\perp(P+m-2)}_{P+m-1} = \mathbf{\Pi}^{\perp}_{\mathbf{U}_{(P+m-2)}} \mathbf{u}_{P+m-1}$ represents the component of $\mathbf{u}_{P+m-1}$ orthogonal to the space spanned by the columns of $\mathbf{U}_{(P+m-2)}$. Similarly, this may be recursively updated by using (for $m \geq 3$)

$$\mathbf{u}^{\perp(P+m-2)}_{P+m-1} = \mathbf{u}^{\perp(P+m-3)}_{P+m-1} - \frac{\mathbf{u}^{\perp(P+m-3)}_{P+m-2} \mathbf{u}^{\perp(P+m-3)H}_{P+m-2} \mathbf{u}^{\perp(P+m-3)}_{P+m-1}}{\|\mathbf{u}^{\perp(P+m-3)}_{P+m-2}\|^2} \tag{27}$$

but

$$\mathbf{u}^{\perp(P)}_{P+m-1} = \mathbf{u}_{P+m-1} - \mathbf{U}_{(P)} \mathbf{R}_P \mathbf{U}^H_{(P)} \mathbf{u}_{P+m-1} \tag{28}$$

In general, to update $\mathbf{u}^{\perp(P+k)}_{P+m-1}$ we use (29), shown at the top of the next page. Now, using (26) and (29), we can recursively update the binary GLR statistic of (23) when testing $\mathcal{H}_m$ against $\mathcal{H}_{m-1}$. Based on this, it is referred to as Forward and Recursive BH-GLRT(FR-BH-GLRT)-based algorithm in the sequel.

C. Parallel Implementation of FR-BH-GLR Detector

To give a desired integration gain in PR systems, N takes a large value. This means that direct implementation of the FR-BH-GLR detector, which works with whole signal at once, seems to be impractical in the PR systems due to the dramatically large number of observation samples. In the following, we will show that the parallel implementation of the FR-BH-GLR detector has the capability to be executed on parallel platforms such as CUDA graphic cards. To perform this, we can rewrite (23) as

$$i_m(n,f) = \frac{|\sum_{r=1}^{R} \mathbf{s}_r^H \mathbf{x}_r^{\perp(P+m-1)}|^2}{\sum_{r=1}^{R} \|\mathbf{p}_r\|^2 \sum_{r=1}^{R} \|\mathbf{x}_r^{\perp(P+m-1)}\|^2} \tag{30}$$

where, the N-dimensional vectors $\mathbf{s}$, $\mathbf{p}$ and $\mathbf{x}^{\perp(P+m-1)}$ are partitioned into R subvectors with dimension $L \times 1$ as [2] $\mathbf{s} = [\mathbf{s}_1^T, ..., \mathbf{s}_R^T]^T$, $\mathbf{p} = [\mathbf{p}_1^T, ..., \mathbf{p}_R^T]^T$ and $\mathbf{x}^{\perp(P+m-1)} = [\mathbf{x}_1^{\perp(P+m-1)^T}, ..., \mathbf{x}_R^{\perp(P+m-1)^T}]^T$. From (26), we have

$$\mathbf{x}_r^{\perp(P+m-1)} = \mathbf{x}_r^{\perp(P+m-2)} - \frac{\sum_{i=1}^{R} [\mathbf{u}^{\perp(P+m-2)}_{P+m-1}]_i{}^H \mathbf{x}_i^{\perp(P+m-2)}}{\sum_{i=1}^{R} [\mathbf{u}^{\perp(P+m-2)}_{P+m-1}]_i{}^H [\mathbf{u}^{\perp(P+m-2)}_{P+m-1}]_i} [\mathbf{u}^{\perp(P+m-2)}_{P+m-1}]_r \tag{31}$$

but

$$\mathbf{x}_r^{\perp(P)} = \mathbf{x}_r - [\mathbf{U}_{(P)}]_r \mathbf{R}_P \sum_{i=1}^{R} [\mathbf{U}_{(P)}]_i{}^H \mathbf{x}_i \tag{32}$$

where $\mathbf{x} = [\mathbf{x}_1^T, ..., \mathbf{x}_R^T]^T$, $\mathbf{u}^{\perp(P+m-2)}_{P+m-1} = \big[[\mathbf{u}^{\perp(P+m-2)}_{P+m-1}]_1^T, ..., [\mathbf{u}^{\perp(P+m-2)}_{P+m-1}]_R^T\big]^T$ and $[\mathbf{U}_{(P)}]_r$ is the rth submatrix with dimension $L \times P$ of matrix $\mathbf{U}_{(P)}$, i.e.,

$$\mathbf{U}_{(P)} = \begin{bmatrix} [\mathbf{U}_{(P)}]_1 \\ [\mathbf{U}_{(P)}]_2 \\ \vdots \\ [\mathbf{U}_{(P)}]_R \end{bmatrix} \tag{33}$$

Next, we use (29) to find (34), shown at the top of the next page, where the vectors $\mathbf{u}^{\perp(P+k-q)}_{P+m-j}$ and $\mathbf{u}_{P+m-1}$ may be presented in the block form of $\mathbf{u}^{\perp(P+k-q)}_{P+m-j} = \big[[\mathbf{u}^{\perp(P+k-q)}_{P+m-j}]_1^T, ..., [\mathbf{u}^{\perp(P+k-q)}_{P+m-j}]_R^T\big]^T$ and $\mathbf{u}_{P+m-1} = \big[[\mathbf{u}_{P+m-1}]_1^T, ..., [\mathbf{u}_{P+m-1}]_R^T\big]^T$. From the representation of (30), it is clear that all vectors are partitioned into R non-overlapping sequences of length L and the total length of each vector is equal to N = RL. In a similar way, matrix $\mathbf{U}_{(P)}$ is partitioned into R non-overlapping row matrices of dimension $L \times P$. As a result, it is possible to execute calculations for each segment on a separate processor. Afterwards, the results of each segment are summed in one of processors. Hence, the new binary hypothesis detector is a parallel implementation (PI) of FR-BH-GLR detector, named PI-FR-BH-GLRT.

D. FFT-Based Implementation of PI-FR-BH-GLR Detector

Since the delay-Doppler coordinates of interested targets are unknown, we need to compute the test statistic $i_m(n,f)$ for a desired *delay-Doppler map*, in which $n = 1, ..., N_d$ with N_d being the time delay index corresponding to the maximum relative bistatic range of interest, and $|f| < f_{max}$ with f_{max} being the maximum Doppler frequency of the interested targets. In practice, this can be implemented very efficiently by fast Fourier transform (FFT) as follows

$$\mathbf{i}_a(\mathbf{x}^{\perp(P+m-1)}, n) = \frac{\mathbf{f}_n(\mathbf{x}^{\perp(P+m-1)}) \odot \mathbf{f}_n(\mathbf{x}^{\perp(P+m-1)})^*}{\sum_{r=1}^{R} \|\mathbf{y}_r^{(n)}\|^2 \sum_{r=1}^{R} \|\mathbf{x}_r^{\perp(P+m-1)}\|^2} \tag{35}$$

[2] N is considered a multiple integer of L.

This article has been accepted for publication in a future issue of this journal, but has not been fully edited. Content may change prior to final publication. Citation information: DOI 10.1109/TSP.2017.2666778, IEEE Transactions on Signal Processing

$$\mathbf{u}_{P+m-1}^{\perp(P+k)} = \begin{cases} \mathbf{u}_{P+m-1} - \mathbf{U}_{(P)}\mathbf{R}_P\mathbf{U}_{(P)}^H\mathbf{u}_{P+m-1} & k=0 \\ \mathbf{u}_{P+m-1}^{\perp(P+k-1)} - \frac{\mathbf{u}_{P+m-2}^{\perp(P+k-1)}\mathbf{u}_{P+m-2}^{\perp(P+k-1)H}\mathbf{u}_{P+m-1}^{\perp(P+k-1)}}{\|\mathbf{u}_{P+m-2}^{\perp(P+k-1)}\|^2} & k=1,...,m-2 \end{cases} \quad (29)$$

$$[\mathbf{u}_{P+m-1}^{\perp(P+k)}]_r = \begin{cases} [\mathbf{u}_{P+m-1}]_r - [\mathbf{U}_{(P)}]_r\mathbf{R}_P\sum_{i=1}^R [\mathbf{U}_{(P)}]_i{}^H[\mathbf{u}_{P+m-1}]_i & k=0 \\ [\mathbf{u}_{P+m-1}^{\perp(P+k-1)}]_r - \frac{\sum_{i=1}^R [\mathbf{u}_{P+m-2}^{\perp(P+k-1)}]_i{}^H[\mathbf{u}_{P+m-1}^{\perp(P+k-1)}]_i}{\sum_{i=1}^R [\mathbf{u}_{P+m-2}^{\perp(P+k-1)}]_i{}^H[\mathbf{u}_{P+m-2}^{\perp(P+k-1)}]_i}[\mathbf{u}_{P+m-2}^{\perp(P+k-1)}]_r & k=1,...,m-2 \end{cases} \quad (34)$$

where $\mathbf{y}^{(n)} = [\mathbf{y}_1^{(n)T}, ..., \mathbf{y}_R^{(n)T}]^T$, and $\mathbf{f}_n(\mathbf{x}^{\perp(P+m-1)}) = FFT\Big(\mathbf{y}^{(n)*} \odot \mathbf{x}^{\perp(P+m-1)}, N_f\Big)$ denotes an N_f-point FFT of the vector $\mathbf{y}^{(n)*} \odot \mathbf{x}^{\perp(P+m-1)}$. As a result, we can define matrix $\mathbf{I}_a(\mathbf{x}^{\perp(P+m-1)}) = [\mathbf{i}_a(\mathbf{x}^{\perp(P+m-1)}, 1), ..., \mathbf{i}_a(\mathbf{x}^{\perp(P+m-1)}, N_d)]$ with dimension $N_f \times N_d$ referred to as a range-Doppler map with N_f Doppler bins and N_d range bins. In this case, the kth Doppler bin corresponds to the Doppler frequency of $f_k = -\frac{f_s}{2} + (k-1)\frac{f_s}{N_f}$ for $k = 1, ..., N_f$, and the relative bistatic range corresponding to the nth range bin is $R_n = \frac{cn}{f_s}$, where c is the speed of light. In the denominator of (35), we also approximate vector $\mathbf{p}$ with $\mathbf{y}^{(n)}$ in order to further reduce the computational complexity of the proposed detection algorithm. In this case, subscript 'a' is used to emphasis on this approximation, which is a reasonable approximate for target detection as shown in [15].

In actual practice, the Doppler frequencies of the interested targets are much lower than the sampling frequency (f_s), so it is possible to employ a decimation technique to reduce the excessive processing load of calculating the N_f-point FFT with almost no loss in signal processing gain [29]. The cascaded integrator-comb(CIC) is a very efficient implementation of a decimation filter [30]- [31]. After applying a CIC filter, the decimated signal is low-pass filtered in order to remove the signal components out of the desired frequency band. Finally, the N_f-point FFT can be replaced by the N_F-point FFT, where $N_F = \frac{N_f}{D}$ and $D \geq 1$ is a decimation factor described in [29]. As such, the number of range-Doppler bins of the matrix $\mathbf{I}_a(\mathbf{x}^{\perp(P+m-1)})$ to be examined may be reduced to $D_d = N_F N_d$ rather that $D_d = N_f N_d$ [see eq.(22)].

From the proposed PI-FR-BH-GLRT-based algorithm it is seen that when a target is detected, it will be considered as an interfering target in the next target detection stage, and it should be removed to detect new targets. After ending the PI-FR-BH-GLRT-based algorithm, the number of radar targets been detected, say M, and their locations in delay and Doppler have been identified. A summary of the proposed detection algorithm is provided in Table I.

TABLE I
SUMMARY OF THE PROPOSED DETECTION ALGORITHM

Input: Threshold η, received vector $\mathbf{x}$, and clutter signature matrix $\mathbf{H}$;

1) **Initialization:**
   - Set threshold η as (22), $m = 0$ and partition the vector $\mathbf{x}$ as $\mathbf{x} = [\mathbf{x}_1^T, ..., \mathbf{x}_R^T]^T$.
2) **Cancellation of direct signal and clutter:**
   - Calculate $\mathbf{R}_P = (\mathbf{U}_{(P)}{}^H\mathbf{U}_{(P)})^{-1}$ where $\mathbf{U}_{(P)} = \mathbf{H}$;
   - Calculate $\mathbf{x}_r^{\perp(P)} = \mathbf{x}_r - [\mathbf{U}_{(P)}]_r\mathbf{R}_P\sum_{i=1}^R [\mathbf{U}_{(P)}]_i{}^H\mathbf{x}_i$ for $r = 1, ..., R$.
3) **Successive target detection:**
   While $\max_{n,k} \mathbf{I}_a(\mathbf{x}^{\perp(P+m)}) > \eta$; **then**
   - Increase m by 1;
   - Find and save the MLE of Delay-Doppler coordinate of the mth target, say (n_m, f_m), which is the location of the maximum of $\mathbf{I}_a(\mathbf{x}^{\perp(P+m)})$;
   - Construct $\mathbf{u}_{P+m} = (\mathbf{y}^{(n_m)} \odot \mathbf{e}^{(f_m)})$, and partition it as $\mathbf{u}_{P+m} = \big[[\mathbf{u}_{P+m}]_1^T, ..., [\mathbf{u}_{P+m}]_R^T\big]^T$.
   - Calculate $[\mathbf{u}_{P+m}^{\perp(P)}]_r = [\mathbf{u}_{P+m}]_r - [\mathbf{U}_{(P)}]_r\mathbf{R}_P\sum_{i=1}^R [\mathbf{U}_{(P)}]_i{}^H[\mathbf{u}_{P+m}]_i$;
   - **for** $k = 1 : m-1$
     Calculate $[\mathbf{u}_{P+m}^{\perp(P+k)}]_r = [\mathbf{u}_{P+m}^{\perp(P+k-1)}]_r - \frac{\sum_{i=1}^R [\mathbf{u}_{P+m-1}^{\perp(P+k-1)}]_i{}^H[\mathbf{u}_{P+m}^{\perp(P+k-1)}]_i}{\sum_{i=1}^R [\mathbf{u}_{P+m-1}^{\perp(P+k-1)}]_i{}^H[\mathbf{u}_{P+m-1}^{\perp(P+k-1)}]_i}[\mathbf{u}_{P+m-1}^{\perp(P+k-1)}]_r$
     end
   - Calculate $\mathbf{x}_r^{\perp(P+m)} = \mathbf{x}_r^{\perp(P+m-1)} - \frac{\sum_{i=1}^R [\mathbf{u}_{P+m}^{\perp(P+m-1)}]_i{}^H\mathbf{x}_i^{\perp(P+m-1)}}{\sum_{i=1}^R [\mathbf{u}_{P+m}^{\perp(P+m-2)}]_i{}^H[\mathbf{u}_{P+m}^{\perp(P+m-1)}]_i}[\mathbf{u}_{P+m}^{\perp(P+m-1)}]_r$; where $r = 1, ..., R$ and $\mathbf{x}^{\perp(P+m)} = [\mathbf{x}_1^{\perp(P+m)T}, ..., \mathbf{x}_R^{\perp(P+m)T}]^T$.

end while

Output: Locations of the radar targets in delay and Doppler.

IV. Analytical Performance Evaluation

In a similar way as finding false alarm probability, we first compute the detection probability of the mth target defined as the probability that the maximum of the delay-Doppler map occurs in the correct bin (n_m, f_m) when the mth target is present. With this definition we have

$$p_d^{(m)'} = Pr\{2Ni_m(n_m, f_m) > \eta' | \mathcal{H}_m\} \quad (36)$$

when $2Ni_m(n_m, f_m) \sim \mathcal{X}_2^2$ or $Ni_m(n_m, f_m) \sim \chi_1^2$. Hence, for this case $p_d^{(m)'}$ may be asymptotically obtained as

$$p_d^{(m)'} = e^{-(\delta_m + \frac{\eta'}{2})}\sum_{k=0}^{\infty}\left(\frac{\delta_m^k}{k!}\sum_{n=0}^{k}\frac{[\frac{\eta'}{2}]^n}{n!}\right) \quad (37)$$

where $\delta_m = \frac{|\alpha_m|^2}{\sigma^2}\|\mathbf{\Pi}_{\mathbf{U}_{(P+m-1)}}^{\perp}\mathbf{s}(n_m, f_m)\|^2$. Making use of (22), we have finally that

$$p_d^{(m)} = e^{-(\delta_m + \ln(\frac{\zeta D_d}{p_{fa}}))}\sum_{k=0}^{\infty}\left(\frac{\delta_m^k}{k!}\sum_{l=0}^{k}\frac{[\ln(\frac{\zeta D_d}{p_{fa}})]^l}{l!}\right) \quad (38)$$

It should be noted that the detection probability of the mth target is an increasing function of δ_m. Based on this, if $SNR_m = \frac{|\alpha_m|^2}{\sigma^2}$ is referred to as the input SNR of the mth target, then $G_m = \|\mathbf{\Pi}^{\perp}_{\mathbf{U}_{(P+m-1)}}\mathbf{s}(n_m, f_m)\|^2$ may be considered as the SNR gain of the mth target provided by the proposed detector. Since $\mathbf{\Pi}^{\perp}_{\mathbf{U}_{(P+m-1)}}$ is an idempotent matrix, it can be concluded that $0 \leq G_m \leq \|\mathbf{s}(n_m, f_m)\|^2$. This means that the mth target may experience a big loss when its delay-Doppler coordinate is near to that of the interference signals including clutter and previously detected targets. In contrast, G_m may take its maximum $\|\mathbf{s}(n_m, f_m)\|^2$ (known as maximum integration gain) in the delay-Doppler coordinates far from that of the interference signals. Based on this, we can define detection loss experienced by the mth target, given by

$$\mathrm{DL}_m = \frac{\|\mathbf{\Pi}^{\perp}_{\mathbf{U}_{(P+m-1)}}\mathbf{s}(n_m, f_m)\|^2}{\|\mathbf{s}(n_m, f_m)\|^2} \tag{39}$$

Note that DL_m depends on the target under test position denoted by (n_m, f_m), the positions of previously detected targets and the characteristics of opportunity signal used for PR detection.

V. Simulation Results and Discussions

In this section, first we evaluate the performance of the proposed PI-FR-BH-GLRT-based algorithm when exploited for both FM and DVB-T based bistatic PRs. Then, the detection performance of the proposed method is compared with other existing methods. For the FM-based bistatic PR, we consider an FM signal with 100 MHz carrier frequency, 100kHz transmitter bandwidth and sampling frequency of 200kHz for both the reference and surveillance channels. For DVB-T signal, we consider 8k DVB-T signal with 600 MHz carrier frequency, 8MHz bandwidth, sampling frequency of 9.1429 MHz, code rate of $\frac{2}{3}$, constellation of "64-QAM" and a cyclic prefix ratio of $\frac{1}{8}$. For FM and DVB-T -based PR systems an integration time of 0.8s and 28ms are considered, respectively. Other parameters such as R, N_f, N_F, D, N_d and D_d are set, respectively, equal to 32, 524288, 2048, 256, 60 and 56242 for the FM signal, while they are considered equal to 32, 524288, 256, 2048, 2743 and 373184 when using the DVB-T signal. Also, to see the effect of time-varying nature of FM signals on threshold setting and target detection performance, we consider two FM signals named as FM S_1 and S_2 signals with auto-ambiguity functions as shown in Fig.1.

In our simulations, we consider direct signals with input direct signal-to-noise ratio (DNR_i)of about 60. Also, ten clutter spikes with zero Doppler and relative bistatic ranges between 0 and 55 km are considered with different input clutter-to-noise ratios (CNR_i) over the interval $5dB \leq \mathrm{CNR}_i \leq 45dB$. Note that the clutter cancellation capability of the proposed detector is similar to the detector presented in [15], hence, the interested reader is referred to [15], for more performance curves, analyses, and discussions which are not repeated here in the interest of brevity.

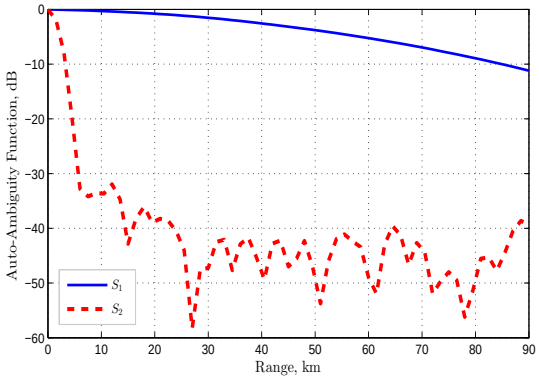

Fig. 1. Auto-ambiguity function at zero velocity for the FM S_1 and S_2 signals corresponding to the silence and music voice track of an FM radio waveform, respectively.

A. Performance of the Proposed Detector

Here, extensive simulation results for both FM and DVB-T based passive radars are presented to demonstrate the effectiveness of the proposed detection algorithm. First, to demonstrate the validity of the asymptotic theoretical results presented in section III, Fig.2 presents estimated false alarm probability of the proposed detector against the predefined false alarm probability p_{fa} for different values of parameter ζ. The estimated false alarm probability, denoted here by P_{fa}, is obtained from 10^8 Monte Carlo simulation runs. We can observe that P_{fa} is very close to the asymptotic ones calculated from (22) when $P_{fa} < 10^{-2}$. For these results we use $D_d = N_F N_d$ and the parameter ζ in (22) is set equal to 0.125 and 0.83 when using the FM S_1 and S_2 signals, respectively. In reality, since the transmitted waveforms are not within the control of the radar designer, it makes sense to calculate the threshold η based on the closed-form solution derived in (22) with $\zeta = 0.83$. As such, we could claim that we have designed a detector with the false alarm probability of level p_{fa} and not of size p_{fa}. Generally, a detector is said to have a false alarm probability of level (size) p_{fa} when the estimated false alarm probability (P_{fa}) satisfies $P_{fa} \leq p_{fa}$ ($P_{fa} = p_{fa}$) [32]. This means that for FM-based PR with time-varying waveforms, designing a constant false alarm rate (CFAR) detector, with respect to the opportunity signals received over different CPIs, is not easily accessible, but it has a controlled false alarm probability. Based on this finding, in the following paragraphs, the threshold η is set equal to 49.05 based on (22) with $\zeta = 0.83$ to attain $P_{fa} \leq 10^{-6}$, i.e. the proposed detector has a level of 10^{-6} when using the FM S_1 signal, while it has a size of 10^{-6} when using the FM S_2 signal, as shown in Fig.2. This is the first contribution of the present work with respect to my previous work presented in [15]. For DVB-T signal, we demonstrate both the asymptotic and estimated false alarm probability in Fig.2 (b). This figure supports our argument on the close relationship between asymptotic and actual false alarm probability of the proposed detector with parameter $\zeta = 1$ for $P_{fa} < 10^{-1}$. Due to the noise-like and approximately the time-invariant nature of DVB-T signals,

This article has been accepted for publication in a future issue of this journal, but has not been fully edited. Content may change prior to final publication. Citation information: DOI 10.1109/TSP.2017.2666778, IEEE Transactions on Signal Processing

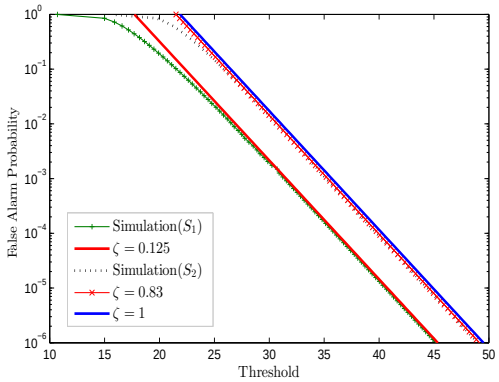

(a) FM S_1 and S_2 signals

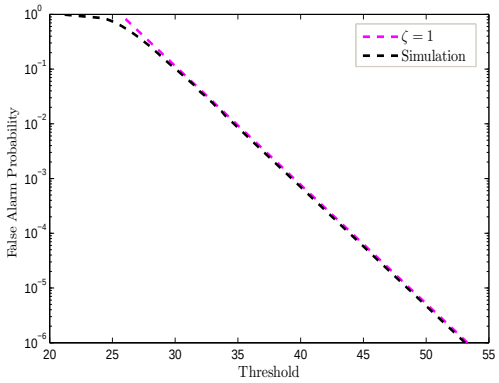

(b) DVB-T signal

Fig. 2. Accuracy of threshold setting is investigated with respect to the corresponding false alarm probability given in (22) for (a) FM S_1 and S_2 signals (b) DVB-T signal.

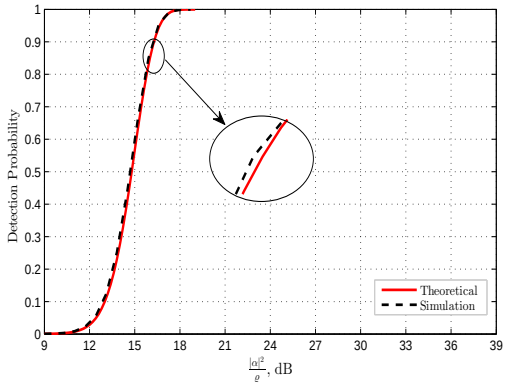

(a) FM S_1 and S_2 signals

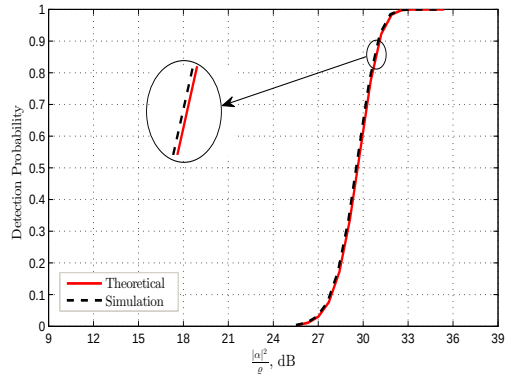

(b) DVB-T signal

Fig. 3. Detection probability as a function of $\frac{|\alpha|^2}{\varrho}$ for $p_{fa} = 10^{-6}$ in a single-target scenario when using (a) FM signal (b) DVB-T signal. For FM and DVB-T -based PBR system integration times of 0.8s and 28ms are considered, respectively.

we can say that the proposed detector has CFAR property with respect to the different opportunity signals received over different CPIs of a DVB-T-based PR system.

In the sequel, we investigate the accuracy of the analytic formula for the detection probability when using the FM and DVB-T signals through numerical examples for $p_{fa} = 10^{-6}$. In this case, the numerical results are obtained from 10^4 Monte Carlo simulation trials. In this case, we demonstrate both the asymptotic and numerical detection probability of the proposed detector for the FM and DVB-T signals in Fig.3 (a) and (b), respectively. Fig.3 shows the detection probability as a function of $\frac{|\alpha|^2}{\varrho}$ with ϱ being the noise power per unit bandwidth, setting equal to $-197dB/Hz$ for both FM and DVB-T based PRs. It can be seen that the estimated detection probability of the proposed test is very close to the asymptotic one, denoted as $p_d^{(1)}$ calculated from (38) with $\mathbf{U}_{(P)} = \mathbf{H}$, in a single-target scenario (STS). By comparing the results of Fig.3 (a) and (b), it is concluded that an FM-based PR system offers better detection performance (about 14.7dB) as compared to that of DVB-T- based PR system thanks to the higher integration time used for FM-based PR system. It should be noted that, for the single-target scenario, the detection performance result using the FM S_1 signal is the same as for the FM S_2 signal.

To examine the ability of the proposed algorithm in multi-target scenario (MTS), we define a scenario, including five targets with characteristics listed in Table II. In this multi-target scenario, the performance of the PI-FR-BH-GLRT algorithm for the FM and DVB-T signals are shown in Figs. 4 and 5. In these figures, symbols $+$, $\square$ are used to indicate the original target positions and estimate of target positions by the PI-FR-BH-GLRT algorithm, respectively. Using the FM S_1 signal, as shown in Fig.4(a), the targets T_2, T_3, T_4 and T_5 are correctly resolved and positioned. In this scenario, the targets T_1 and T_2 are placed at the same doppler frequency, but in different relative bistatic ranges. We see that the poor range resolution of the considered FM signal yields into a big loss for detecting target T_1 in the presence of the target T_2 with higher power as compared to the target T_1. For the FM S_2 signal, we can observe that all the targets are correctly resolved and positioned as shown in Fig.4(b). Form Fig.5, it is observed that, for the DVB-T signal, the targets T_1, T_2, T_4 and T_5 are correctly resolved and positioned. In this case, poor frequency resolution of the DVB-T signal as compared to that of FM signal leads to the missing of the target T_3, which is in the same relative bistatic range as T_4, but with lower power as compared to the target T_4.

This article has been accepted for publication in a future issue of this journal, but has not been fully edited. Content may change prior to final publication. Citation information: DOI 10.1109/TSP.2017.2666778, IEEE Transactions on Signal Processing

TABLE II
TARGETS CHARACTERISTICS IN THE CONSIDERED MULTI-TARGET SCENARIO

Targets	T_1	T_2	T_3	T_4	T_5
Bistatic Range (km)	10	13	45	45	54.79
Bistatic Velocity (m/s)	91.55	91.55	-117.7	-122.07	135.15
SNR$_i$ (dB)	-27	-3	-28	-8	-17

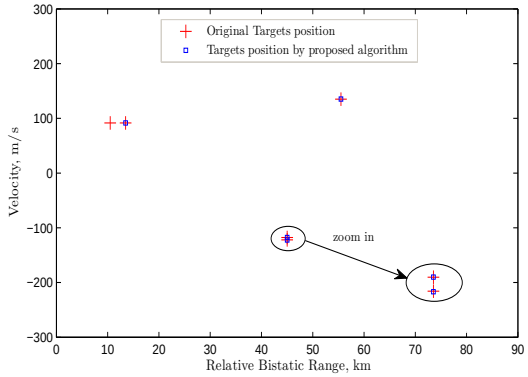

(a) FM S_1 signal

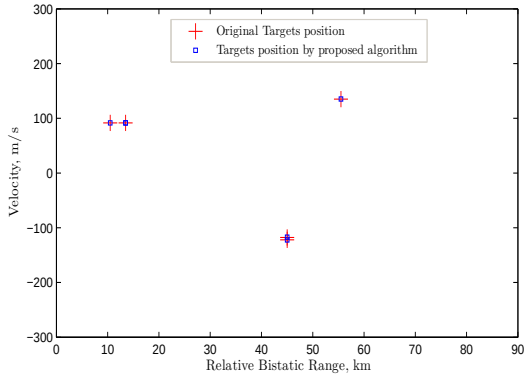

(b) FM S_2 signal

Fig. 4. Effectiveness evaluation of the PI-FR-BH-GLRT-based algorithm over sketch of surveillance signal contribution in desired delay-Doppler plane for multi-target scenario with targets characteristics listed in Table II for $p_{fa} = 10^{-6}$ for FM S_1 and S_2 signals.

In order to get further insight into target detection using the FM and DVB-T signals, we depicts detection probability $p_d^{(m)}$ for $m = 1, ..., 5$ as a function of $\frac{|\alpha|^2}{\varrho}$ for all the targets in the considered multi-target scenario. To do this, we change the value of $\frac{|\alpha|^2}{\varrho}$ corresponding to the mth testing target, T_m say, in the presence of the other targets known as interfering targets, whose their $\frac{|\alpha|^2}{\varrho}$s and their positions are listed in Table II. For this case, input SNR can be defined as $\frac{|\alpha|^2}{\varrho}$ divided by the sampling frequency f_s, i.e., SNR$_i = \frac{|\alpha|^2}{\varrho f s}$. The results of this simulation for FM and DVB-T signals are reported in Figs.6 and 7, respectively. From Fig. 6, it is seen that different targets T_m for $m = 1, ..., 5$ have not the same performance due to the different characteristic of the considered FM signals. For the FM S_1 signal, the targets T_3, T_4 and T_5 follow the performance of the proposed detector in the single target

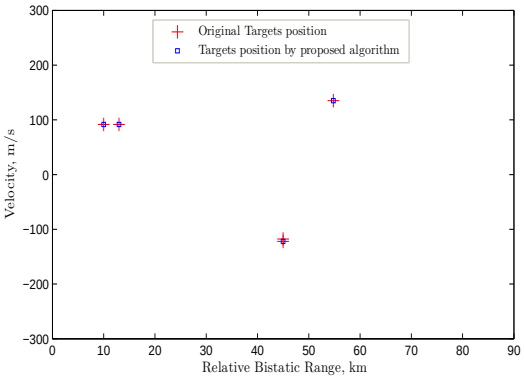

Fig. 5. Effectiveness evaluation of the PI-FR-BH-GLRT-based algorithm over sketch of surveillance signal contribution in desired delay-Doppler plane for multi-target scenario with targets characteristics listed in Table II for $p_{fa} = 10^{-6}$ for DVB-T signal.

scenario, while the target $T_1(T_2)$ experiences a performance loss of about 17.6dB in the presence of the target $T_2(T_1)$ for detection probability of 0.9 when compared with the results of single target scenario shown in Fig.3 (a). Using the FM signal S_2 reduces this loss to about 3dB because of the better signal characteristic of the FM S_2 signal as compared to that of S_1 signal[see Fig.1]. In the case of the DVB-T signal, as shown in Fig. 7, the targets T_1, T_2 and T_5 follow the performance of the proposed detector in the single target scenario, whereas target $T_3(T_4)$ experiences a performance loss of about 2.5dB in the presence the target $T_4(T_3)$. To explain this, it is interesting to evaluate the detection loss (DL) experienced by different targets as defined in (39). To do so, for the FM S_1 signal, we plot DL versus the relative bistatic range as shown in Fig. 8, while for the DVB-T signal we depict DL versus the bistatic velocity as shown in Fig. 9. In both cases, we assume that an interfering target is placed in the zero relative bistatic range and the zero velocity for convenience. Generally speaking, the detection loss experienced by the mth target depends on the delay-Doppler coordinate of the mth target, the characteristics of the opportunity signal used for detection, and also the delay-Doppler coordinates of the targets detected in previous steps of the algorithm. Thus, the curve of DL versus bistatic range (Doppler) can be referred to as range-dimension loss profile (Doppler-dimension loss profile) and may be used for justifying the losses experienced by different targets shown in Fig.6.

B. Performance Comparison to Existing PR detection Algorithms

In the following, our purpose is to compare the detection performance of the proposed detector with other existing methods. Among them, the detection algorithms of [11] and [15] are the main reference comparison for FM-based PRs, while we consider the detector presented in [5] for DVB-T-based PRs. The performance comparison of these detectors with other existing methods can also be found in [15], [16] and [35]. We begin by considering an FM-based PBR system with the multi-target scenario of Table II. In [11],

This article has been accepted for publication in a future issue of this journal, but has not been fully edited. Content may change prior to final publication. Citation information: DOI 10.1109/TSP.2017.2666778, IEEE Transactions on Signal Processing

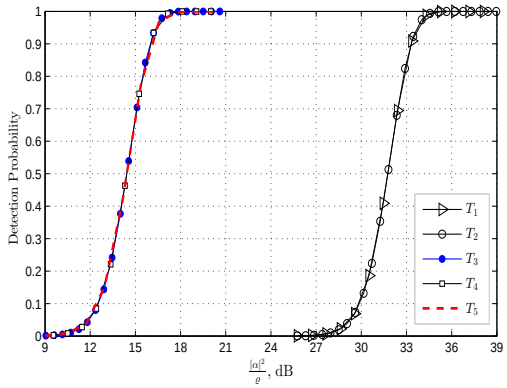

(a) FM S_1 signal

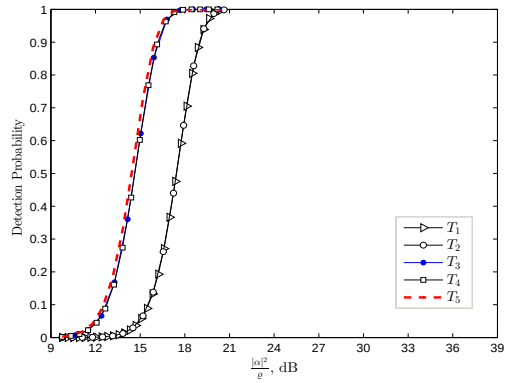

(b) FM S_2 signal

Fig. 6. Detection performance of the PI-FR-BH-GLRT-based algorithm as a function of $\frac{|\alpha|^2}{\varrho}$ for the FM S_1 and S_2 signals in the multi-target scenario with targets characteristics listed in Table II for $p_{fa} = 10^{-6}$.

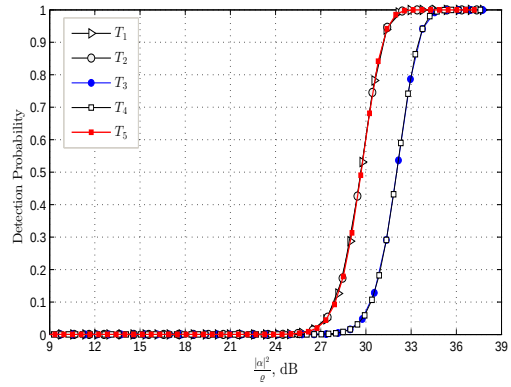

Fig. 7. Detection performance of the PI-FR-BH-GLRT-based algorithm as a function of $\frac{|\alpha|^2}{\varrho}$ for the considered DVB-T signal in the multi-target scenario with targets characteristics listed in Table II for $p_{fa} = 10^{-6}$.

a multistage processing algorithm for disturbance removal and strong targets detection based on projections of the received signal in a subspace orthogonal to both the disturbance and previously detected targets was presented. Then, a cell-averaging CFAR detector was applied to the cross-ambiguity function (CAF) of the cleaned signal to detect weak targets. Here, the detector proposed in [11] is referred to as the

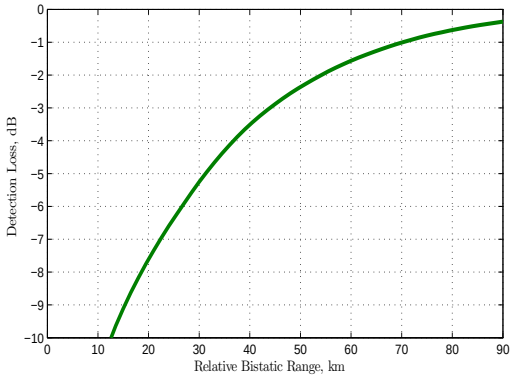

Fig. 8. DL versus relative bistatic range at the zero Doppler when using the FM S_1 signal for detection.

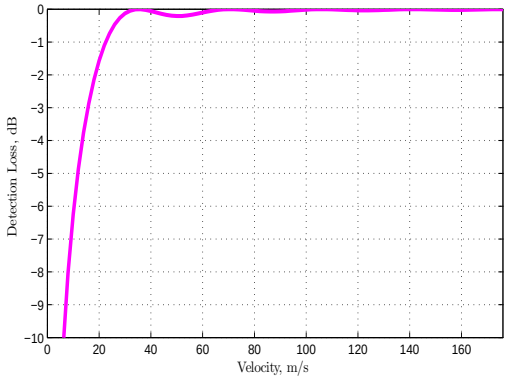

Fig. 9. DL versus bistatic Doppler frequency when using DVB-T signal.

multistage processing (MP) and cell-averaging(CA) detection algorithm, abbreviated as MP-CA detector. Throughout the paper, the CA detector is configured with a total number of training bins equal to 120, and two guard cells on each side of the test cell are also used to prevent from the self-masking effect [11]. Other parameters of the MP-CA detector are the same as those used in [11] (e.g., $\varepsilon = 3dB$ and $\eta = 5dB$). The detection performance of the MP-CA detector when using the FM S_2 signal is presented in Fig.10. By comparing Figs. 6 (b) and 10, for the FM S_2 signal, we can observe that the detection performance of the proposed algorithm is superior to that of the MP-CA detector for all the targets in the considered scenario. Our simulation results show that the disturbance removal part of the MP-CA detector cannot detect target T_1 (T_3) when the target under test is T_2 (T_4), i.e., the MP-CA detector was proposed to only detect and remove strong targets (targets with high input SNR). As a result, the interfering target T_1 (T_3) inevitably increases the threshold of the CA-CFAR detector for detecting the target T_2 (T_4); hence, a severe degradation of the MP-CA detector is seen. This target detection issue is generally known as the capture effect [33]- [34], whereas our proposed algorithm does not have such problems. In this case, the MP-CA detector experiences an additional loss of about 9.7dB, 8.5dB, 16.1

This article has been accepted for publication in a future issue of this journal, but has not been fully edited. Content may change prior to final publication. Citation information: DOI 10.1109/TSP.2017.2666778, IEEE Transactions on Signal Processing

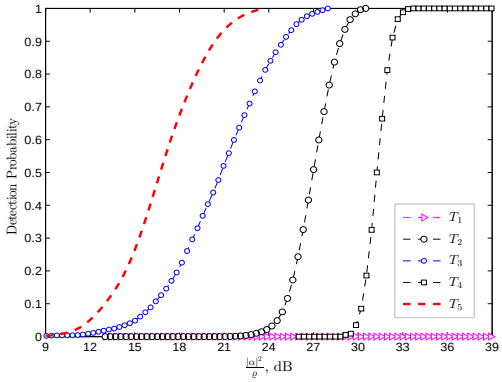

Fig. 10. Detection performance of the MP-CA detector of [11] in the multi-target scenario with targets characteristics listed in Table II for $p_{fa} = 10^{-6}$ when using the FM S_2 signal for detection.

and 4.5 dB as compared with that of the proposed detector for detecting targets T_2 to T_5 at detection probability of 0.9 and $p_{fa} = 10^{-6}$, respectively. Also, the MP-CA detector is unable to detect the target T_1, such as we obtain $p_d^{(1)} = 0$ for $\frac{|\alpha|^2}{\varrho}$ values of between 9dB and 39dB. For the FM S_1 signal with the poor range resolution, the detection probabilities of zero have been obtained for all the targets in the considered scenario for $\frac{|\alpha|^2}{\varrho}$ values between 9dB and 39dB when using the the MP-CA detector. This significant detection loss of the MP-CA detector is related not only to the self-masking effect due to the poor range resolution of the FM S_1 signal but also to the heuristic algorithm used to estimate the noise power in its multistage processing algorithm. As a consequence of our simulations, it is concluded that most conventional collaborative PR detectors estimating the noise variance locally suffer from the self-masking and capture effect, especially in FM-based PR systems with poor ambiguity characteristics.

It is known that digital television transmitters offer a well-defined signal with sufficient bandwidth for reasonable precision in range and are noise-like, thereby allowing for good target detection. However, it was shown in [5] and [12] that the structure of the DVB-T signal has given rise to some deterministic ambiguities (or false targets) consistent in range and Doppler with targets of interest. Since the transmitted signal structure is beyond the control of the passive radar system designer, ambiguities must be managed at the receiver. Authors of work [12] developed a mismatched signal processing approach after applying a pre-processing on both the reference and surveillance channels. This method can be used only to mitigate the effects of the deterministic ambiguities of the DVB-T signal at the price of some signal-to-noise ratio mismatched loss and more computational load. In addition, the signal conditioning algorithm used in the reference channel of this system reduces surveillance clutter cancellation capability, thereby resulting in an excessive false alarm [35]. In [5], a new signal conditioning approach for DVB-T-based PR systems was proposed, able to overcome the limitations of [12] in terms of achievable performance, computational complexity and system requirements. For disturbance (multipath echoes) removal, the extensive cancellation algorithm described in [11] was used. Then, the CA-CFAR threshold was applied on the obtained 2-dimensional range-Doppler cross-correlation function (2D-CCF) between the surveillance and the (possibly mismatched) reference signal to detect weak and strong targets. Here, the detector proposed in [5] is referred to as the extensive cancellation algorithm (ECA) and cell-averaging(CA) detection, denoted as the ECA-CA detector. By comparing the results of Figs.11(a) and 7, we can observe the performance advantage of the proposed method as compared to that of the ECA-CA detector even for DVB-T signal. In this case, the target under test T_4 can be detected with probability of one since the targets T_3 and T_4 cannot be resolved by the ECA-CA detector, so they can be considered as a single target denoted by $T_{3,4}$ with high input SNR yielding detection probability of one. Coming back to Fig. 7, we see that in contrast to the proposed detector, the ECA-CA detector incurs losses of 4.8, 4.9 and 1.4dB for detecting the targets T_1, T_2 and T_5 with detection probability of 0.9 and $p_{fa} = 10^{-6}$. More importantly, as mentioned before, exploiting the proposed detector makes it possible to detect the target T_3 in the presence of the strong interfering target T_4 with a loss of about 2.5dB, whereas this is impossible with the ECA-CA detector due to the capture effect of the strong interfering target T_4. Fig.11 (b) also includes the detection results of applying the MP-CA detector for the DVB-T signal. It is seen that the MP-CA detector provides about the same performance as the ECA-CA detector. This is not totally surprising since the MP-CA detector is based on an intuitive basis, and no intrinsic optimality or pseudo-optimality has been associated with it [15]. For both the FM and DVB-T -based PR cases, our simulation results, not reported here, show that the detection performance of the PI-FR-BH-GLR-based detector matches pretty well with that of the 2S-GLR-based detector presented in [15], while they have been obtained under two different target-detection problems. In the following, we will show that the PI-FR-BH-GLR-based detector is computationally simpler than the 2S-GLR-based algorithm.

Finally, we would like to remark on the computational complexity of various detection algorithms considered in this paper in terms of the number of complex multiplications (CMs). According to the algorithm description of Table I, the number of CMs needed to remove direct signal and clutter from the received signal is $NP^2 + 3NP + \mathcal{O}(P^2 log_2 P) + P^2$ where $N = LR$. For the successive target detection part of the proposed algorithm with Q iterations, $3NN_dQ + 2NPQ + 4NQ + 1.5NQ(Q-1) + QN_dN_F log_2 N_F + QN_F N_d + QP^2 + QN_d + 0.5Q(Q-1) + Q$, CMs are required. Thus, the overall CMs during the Q iteration $(Q \geq M)$ of the proposed detection algorithm is $C_1^{\times} = LRP^2 + 3LRP + \mathcal{O}(P^2 log_2 P) + P^2 + 3NN_dQ + 2NPQ + 4NQ + 1.5NQ(Q-1) + QN_dN_F log_2 N_F + QN_F N_d + QP^2 + QN_d + 0.5Q(Q-1) + Q$. For the 2S-GLR- based detector the overall complex multiplications is $C_2^{\times} = C_1^{\times} + 2NP + 2NQ + 2$. This shows a computational

This article has been accepted for publication in a future issue of this journal, but has not been fully edited. Content may change prior to final publication. Citation information: DOI 10.1109/TSP.2017.2666778, IEEE Transactions on Signal Processing

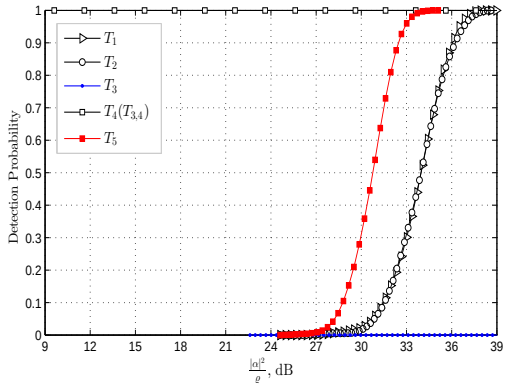

(a) ECA-CA detector

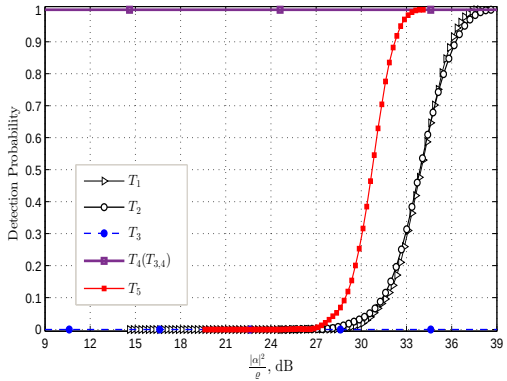

(b) MP-CA detector

Fig. 11. Detection performance comparison of the ECA-CA detector and the MP-CA detector in the multi-target scenario characterized in Table II for $p_{fa} = 10^{-6}$ when using the DVB-T signal for detection.

load saving of about $2NP+2NQ+2$ when using the proposed detector. Similarly, one can show that the ECA-CA detector have complexity $C_3^{\times} = NP^2 + 3NP + \mathcal{O}(P^2 log_2 P) + P^2 + NN_d + N_d N_F log_2 N_F + O(N_F N_d)$. The overall CMs of the MP-CA detector after N_s stages ($N_s \leq Q$) is $C_4^{\times} = C_3^{\times} + N_s(N + N_F log_2 N_F + N_F) + \sum_{i=1}^{N_s}(Nn_i^2 + 4Nn_i + n_i^2)$, where n_i is the number of Doppler-range bins used to update the cancellation mask at the ith stage ($n_i \geq 1$). This parameter depends on the number of Doppler-range bins at which a detection was declared, characteristics of opportunity signal used for detection as well as the SNR levels of the detected targets [11], [15]. By comparing the computational complexity of the considered detection algorithms, it follows that the main computational complexity of these methods depends on term NP^2; hence, they have approximately the same computational complexity of order $\mathcal{O}(NP^2)$. More precisely, the computational complexity of the proposed detector is tolerably higher than the MP-CA detector for FM-based PR systems. However, the tolerable increase in the complexity of the proposed detector can provide 4-16 -dB improvement in the detection performance. For DVB-T- based PR systems, the ECA-CA detector has lower computational complexity than that of the proposed detector, while a detection performance improvement of about 2-5-dB is achievable by using the proposed detection algorithm.

VI. CONCLUSIONS

In conclusion, we model target detection problem in PR systems as an M-ary hypothesis test problem for multi-target scenarios. To this problem, a forward and sequential GLR-based detector was proposed in which the targets are detected sequentially and the previously detected targets are treated as interferences thus allowing the detection of the weakest ones. Furthermore, we propose a parallel implementation of GLR-based detector to reduce the amount of memory required to implement the proposed algorithm. After that, we derive the closed-form expressions for the threshold and detection probability using the asymptotic expression of GLRT statistics. We also study the accuracies of the proposed threshold selection method and detection performance through numerical simulations. Due to dramatically large number of observation sample in PR systems, it was shown that the accuracy of our derived expressions is very high.

Through our simulation results, it was also concluded that the proposed detection algorithm significantly outperformed the existing methods without adding significant complexity to them. This does not mean that it is not possible to develop a heuristic algorithm with smaller computational complexity. What is important to note is that the proposed detector can be considered as a benchmark detector of such cases.

REFERENCES

[1] Howland, P. E.: 'Target tracking using television-based bistatic radar', *IEE Proceedings on Radar, Sonar and Navigation, 146, 3(1999), 166-174.*

[2] Griffiths, H.D., and Baker, C.J.: 'Passive coherent location radar systems. Part 1: performance prediction', *IET Radar, Sonar and Navigation,IEE Proceedings-, 152, 3(2005), 153-159.*

[3] Saini, R., and Cherniakov, M.: 'DTV signal ambiguity function analysis for radar application', *IEE Proceedings on Radar, Sonar and Navigation, 152, 3(June 2005), 133-142.*

[4] Radmard, M., Bastani, M., Behnia, F. and Nayebi, M.M.: 'Cross ambiguity function analysis of the'8k-mode'DVB-T for passive radar application', In 11-th International Radar Symposium, June 2010, 1-4.

[5] Colone, F., Langellotti, D. and Lombardo, P.: 'DVB-T signal ambiguity function control for passive radars', *IEEE Trans.on Aerospace and Electronic Systems, 50, 1(January 2014), 329-347.*

[6] Poullin, D.: 'Passive detection using broadcasters (DAB, DVB) with CODFM modulation', *IEE Proceedings on Radar, Sonar and Navigation, 152, 3(June 2005), 143-152.*

[7] Tan, D., Sun, H., Lui, Y., Lesturgie, M., and Chan, H.: 'Passive radar using global system for mobile communication signal: Theory, implementation and measurements', *IEE Proceedings on Radar, Sonar and Navigation, 152, 3(June 2005), 116-123.*

[8] Evers, A. and Jackson, J.A.: 'Cross-ambiguity characterization of communication waveform features for passive radar', *IEEE Trans.on Aerospace and Electronic Systems, 51, 4(October 2015), 3440-3455.*

[9] Baker, C. J., Griffiths, H. D., and Papoutsis, I.: 'Passive coherent location radar systems. Part 2: Waveform properties', *IEE Proceedings on Radar, Sonar and Navigation, 152, 3(June 2005), 160-168.*

[10] Kulpa, K. S., and Czekala, Z.: 'Masking effect and its removal in PCL radar', *IEE Proceedings on Radar, Sonar and Navigation, 152, 3 (June 2005), 174-178.*

[11] Colone, F., OHagan, D.W., Lombardo, P., and Baker, C. J.: 'A multistage Processing Algorithm for Disturbance Removal and Target Detection in Passive Bistatic Radar', *IEEE Trans.on Aerospace and Electronic Systems, 45, 3(April 2009), 698-722.*

[12] Palmer,J. E., Harms, H. A., Searle, S. J. and Davis, L.: 'DVB-T Passive radar signal processing', *IEEE Trans. On Signal Processing, 61, (2013), 2116-2126.*

[13] Palmer, J. E. and Searle, S. J.: 'Evaluation of adaptive filter algorithms for clutter cancellation in Passive Bistatic Radar', IEEE National Radar Conference, 2012.
[14] Zaimbashi, A.: 'Target Detection in Passive Radars Based on Commercial FM Radio Signals', *P.h.D. thesis, Shiraz University, Iran, 2013.*
[15] Zaimbashi, A., Derakhtian, M., and Sheikhi, A.: 'GLRT-Based CFAR Detection in Passive Bistatic Radar', *IEEE Trans. on Aerospace and Electronic Systems, 49, 1 (January 2013), 134-159.*
[16] Zaimbashi, A., Sheikhi, A. and Derakhtian, M.: 'Evaluation of Detection Performance of Passive Bistatic Radar Detectors based on Commercial FM Radio Signals', Journal of "Radar", 1, 2 (2014), 23-34.
[17] Zaimbashi, A., Derakhtian, M., and Sheikhi, A.: 'Invariant Target Detection in Multiband FM-Based Passive Bistatic Radar', *IEEE Trans. on Aerospace and Electronic Systems, 50, 1 (January 2014), 720-736.*
[18] Zaimbashi, A.: 'Broadband Target Detection Algorithm in FM-Based Passive Bistatic Radar Systems ', *IET Radar, Sonar and Navigation, doi: 10.1049/iet-rsn.2015.0608.*
[19] Zaimbashi, A.: 'Multiband FM-based passive bistatic radar: target range resolution improvement', *IET Radar, Sonar and Navigation, 11, 5 (2016), 20-33.*
[20] Zaimbashi, A.: 'Target detection in FM-Based Passive Radars in the presence of interference signals in reference channel' , Journal of "Radar", 10, 2 (2016), 1-15.
[21] Wang, L. and Yazici, B.: 'Passive Imaging of Moving Targets using Sparse Distributed Apertures', SIAM Journal on Imaging Sciences, Vol.5, No.3, pp. 769-808, 2012.
[22] Wang, L. and Yazici, B.: 'Passive imaging of moving targets exploiting multiplescattering using sparse distributed apertures', Inverse Problems, 28 (2012), 125009(36pp): 1-36.
[23] Wang, L. and Yazici, B.: 'Passive imaging using distributed apertures in multiple-scattering environments', Inverse Problems, 26 (2010), 065002 (37pp):1-37.
[24] Hack, D. E. and Patton, L. K. and Himed, B. and Saville, M. A.: ' Centralized passive MIMO radar detection without direct-path reference signals, *IEEE Trans. On Signal Processing, 62, 11 (2016), 3013-3023.*
[25] Liu, J., Li, H. and Himed, B.: 'Two target detection algorithms for passive multistatic radar', *IEEE Trans. On Signal Processing, 62, 22 (Novmber 2014), 5930-5939.*
[26] Kay, S.M.: Fundamentals of Statistical Signal Processing: Detection Theory, *(PTR Prentice-Hall, Englewood Cliffs, NJ, 1998)*
[27] Zoubir, A.M., Viberg, M., Chellappa, R., and Theodoridis, S.: 'Array and Statistical Signal Processing', Academic Press Library in Signal Processing, 3, (2014), 3-967.
[28] Kay, S.M.: Fundamentals of Statistical Signal Processing: Estimation Theory, *(PTR Prentice-Hall, Englewood Cliffs, NJ, 1993)*
[29] Cherniakov, M.: Bistatic radar: emerging technology, *(Wiley and Sons, 2007).*
[30] Harris, F.J.: 'On the use of windows for harmonic analysis with the discrete fourier transform', *Proc. IEEE, 66, 1(January 1978), 5183.*
[31] Hogenauer, E.B.: 'An economical class of digital filters for decimation and interpolation', IEEE Trans. Acoustics, Speech, and Signal Processing, 29,2 (April 1981), 155162.
[32] Lehman, E.L. and , Romano, J.P.: Testing statistical hypothesis, *(New York: Springer Verlag, 2005).*
[33] Zaimbashi, A., and Norouzi,Y.: 'Automatic Dual Censoring Cell Averaging CFAR Detector in Nonhomogenous Environments' , EURASIP Journal on signal processing, 88,11(November 2008), 2611-2621.
[34] Tao, D., Doulgeris, A.P. and Brekke, C.: 'A Segmentation-Based CFAR Detection Algorithm Using Truncated Statistics', *IEEE Trans. On Geoscience and Remote Sensing , 54, 5 (2016), 2887 - 2898.*
[35] Asadi-poya, A., Derakhtian, M., and Zaimbashi, A.: 'Adaptive clutter cancellation and target detection algorithm in DVB-T-based passive radars', ICEE-21, Ferdowsi University of Mashhad, Mashhad, Iran, May 17-19, 4 (2013), 304-311.

Amir Zaimbashi received the B.Sc. degree in electronics from Shahid Bahonar University, Kerman, Iran, in 2004, and the M.Sc. degree in communication systems from Yazd University, Yazd, Iran, in 2005. From 2006 to 2008, he has worked at Electrical and Computer Engineering Research Center, Isfahan University of Technology, Isfahan, Iran, as a researcher in the field of digital signal processing, and involved in the design and development stages of several communication systems. He received the Ph.D. degree in communication systems from the Shiraz University, Shiraz, Iran, in 2013. Since 2013, he has been with the Department of Electrical Engineering, Shahid Bahonar University of Kerman, Kerman, Iran, where he is currently an Assistant Professor. His research interests include signal detection and estimation and related topics in the areas of signal processing and communications.

Dr. Zaimbashi is a recipient of the 24th Iranian Conference on Electrical Engineering(ICEE) Best Paper Award for a paper on radar target detection. He is frequently a reviewer for IEEE Transactions on Aerospace and Electronic Systems, IEEE Transactions on signal Processing, IEEE Communications Letters, IET Radar, Sonar and Navigation, and other international journals.